THE EUROPEAN
PHYSICAL JOURNAL C

CrossMark

Regular Article - Experimental Physics

Design and implementation of a crystal collimation test stand at the Large Hadron Collider

D. Mirarchi[1,a], **G. Hall**[2], **S. Redaelli**[1], **W. Scandale**[1]

[1] European Organization for Nuclear Research, CERN, 1211 Geneva 23, Switzerland
[2] Blackett Laboratory, Imperial College, London SW7 2AZ, UK

Abstract Future upgrades of the CERN Large Hadron Collider (LHC) demand improved cleaning performance of its collimation system. Very efficient collimation is required during regular operations at high intensities, because even a small amount of energy deposited on superconducting magnets can cause an abrupt loss of superconducting conditions (quench). The possibility to use a crystal-based collimation system represents an option for improving both cleaning performance and impedance compared to the present system. Before relying on crystal collimation for the LHC, a demonstration under LHC conditions (energy, beam parameters, etc.) and a comparison against the present system is considered mandatory. Thus, a prototype crystal collimation system has been designed and installed in the LHC during the Long Shutdown 1 (LS1), to perform feasibility tests during the Run 2 at energies up to 6.5 TeV. The layout is suitable for operation with proton as well as heavy ion beams. In this paper, the design constraints and the solutions proposed for this test stand for feasibility demonstration of crystal collimation at the LHC are presented. The expected cleaning performance achievable with this test stand, as assessed in simulations, is presented and compared to that of the present LHC collimation system. The first experimental observation of crystal channeling in the LHC at the record beam energy of 6.5 TeV has been obtained in 2015 using the layout presented (Scandale et al., Phys Lett B 758:129, 2016). First tests to measure the cleaning performance of this test stand have been carried out in 2016 and the detailed data analysis is still on-going.

1 Introduction

The present collimation system of the LHC [2] has achieved excellent cleaning performance with an inefficiency of about

1×10^{-4} and ensured safe operation without quenches from circulating beam losses with stored beam energies up to 270 MJ at 6.5 TeV [3,4]. Although this performance is very satisfactory, further improvements are deemed necessary for the high-luminosity upgrade (HL-LHC) of the LHC [5–8] that aims at achieving about 700 MJ stored energies. Also note that the halo cleaning efficiency is drastically reduced with heavy ion beams, where a worsening of a factor about 100 is observed with respect to proton beams.

The possibility to use a crystal-based collimation system represents an option for improving both cleaning performance and impedance of the present system (main limitations with HL-LHC beams [9]). Crystal collimation relies on using bent crystals instead of primary collimators to steer halo particles onto one single absorber, as opposed to the present multi-stage collimation system, which is based on massive amorphous blocks of material to intercept halo particles. Experimental results obtained with proton and lead ion beams at the super proton synchrotron (SPS) [10–14] in the framework of the UA9 experiment are very promising. However they are not considered exhaustive enough to propose a crystal collimation scheme as a baseline for future upgrades. A demonstration of this novel scheme in the LHC conditions, in particular a direct comparison of the cleaning efficiency achievable with the two systems, is considered mandatory. Also note that SPS tests were carried out only in static conditions (coasting beams), whereas known LHC limitations require an efficient collimation process throughout the whole operational cycle (injection, ramp, squeeze, collision).

In this paper the design of a crystal collimation system that enables beam tests at the LHC is presented. After an introduction of basic concepts of crystal collimation and a comparison of this novel scheme to the present one, the design goals and constraints for installation into the LHC are discussed. A solution conceived to fulfill all the requirements is presented. Optimized crystal parameter are studied to allow

[a] e-mail: daniele.mirarchi@cern.ch
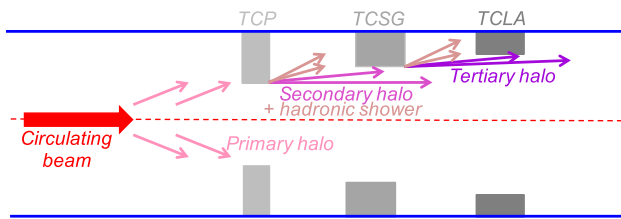
Fig. 1 Working principle of the present collimation system

beam collimation tests in all relevant LHC conditions. Layouts proposed for feasibility tests of crystal collimation at the LHC are then presented. Finally the expected performance, as assessed in simulations, is presented and compared to that of the present LHC collimation system.

The installation of the layouts discussed here was carried out in 2015, in the ring of the LHC beam 1. Preliminary feasibility tests were performed in the first part of Run 2, and the first observation of crystal channeling at the record beam energy of 6.5 TeV was obtained [1]. First tests to measure the cleaning performance of this test stand have been carried out in 2016 and the detailed data analysis is still on-going.

## 2 Multi-stage and crystal-based collimation systems

2.1 LHC multi-stage collimation

An illustrative picture of the working principle of the present collimation system is given in Fig. 1. The present LHC system [2,3] is composed of 44 movable ring collimators per beam, placed in a precise multi-stage hierarchy that must be maintained in any machine configuration to ensure optimal cleaning performance. Two LHC insertions (IR) are dedicated to collimation: IR3 for momentum cleaning, i.e. removal of particles with a large energy offset (cut from $\delta p/p \sim 0.2\%$ for zero betatron amplitude); and IR7 for betatron cleaning, i.e. continuous controlled disposal of transverse halo particles. Each collimator insertion features a three-stage cleaning based on primary collimators (TCP), secondary collimator (TCSG) and absorber (TCLA). In this scheme, the energy carried by the beam halo intercepted by TCPs is distributed over several collimators (e.g. 19 collimators are present in the betatron cleaning insertion). Dedicated collimators for protection of sensitive equipment (such as TCTP for the inner triplets), absorption of physics debris (TCL) and beam dump protection (TCSP) are present at specific locations of the machine. A detailed description of these functionalities goes beyond the scope of this paper and can be found in [2]. The complete collimation layout of the LHC is shown in Fig. 2.

The main limitation of the present system is represented by the level of cleaning inefficiency in the IR7 dispersion suppressor (IR7-DS). Protons experiencing single diffractive interactions in the TCPs are lost at the first dispersive
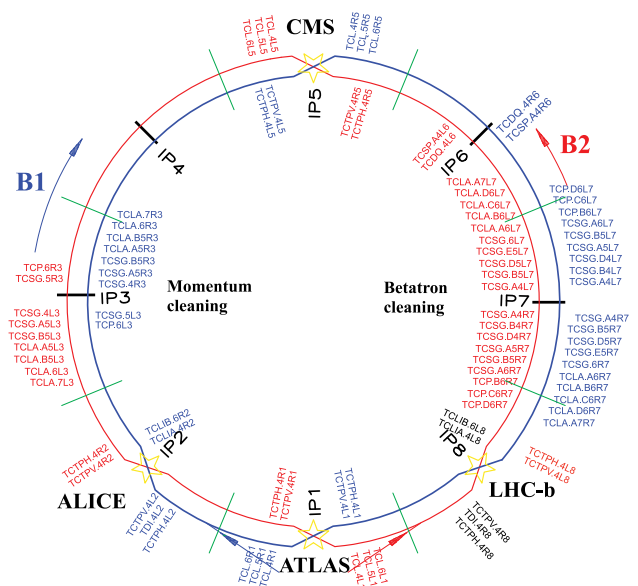
Fig. 2 Collimation layout in the LHC, for both beams
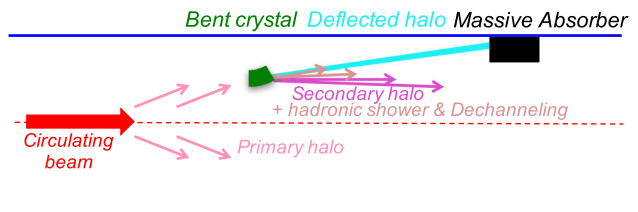
Fig. 3 Working principle of the crystal collimation system

peak arising from the first dipoles downstream of the IR7 straight section (i.e. IR7-DS), because of their momentum offset. These protons are typically not intercepted by TCSGs because of their small transverse scattering angle in the TCPs. A similar limitation occurs for ion beams collimation. Ion fragments produced by the interaction of heavy ions with TCPs are also lost in the IR7-DS [15].

This system requires multiple collimators (11 TCSGs and 5 TCLAs per beam) to catch efficiently the secondary halo out-scattered by the primary collimators. This increases the collimation contribution to the machine impedance, which could lead to beam instabilities.

2.2 Crystal-based collimation

The crystal collimation concept is shown schematically in Fig. 3. It relies on coherent steering of halo particles onto a single massive absorber per plane by using crystal channeling. Ideally, only one crystal per plane is needed, with an associated absorber of channeled particles. Crystals are placed at the edge of the beam envelope as with the present TCPs, and angularly oriented to position the crystalline planes at the entry point parallel to the beam direction. The main advan-

tages of a crystal collimation system are a significant reduction of losses in the IR7-DS and an important decrease of the machine impedance. The present collimation system represents about the 90% of the resistive wall impedance budget of the LHC [16], which is mainly due to the 19 collimators in the IR7. Thus, the fewer collimators surrounding the beam in the case of crystal collimation would lead to a drastic reduction of the resistive wall impedance of the entire machine.

The improved cleaning performance is mainly due to the reduced inelastic interaction rate at the crystal compared to TCPs. Channeled particles travel in a relatively empty space between crystalline planes. Moreover, the deflection given to channeled particles is defined by the crystal bending. Therefore, large bending leads to large impact parameter on the absorber, increasing its effective length seen by the impacting particles and therefore reducing out-scattered protons that could emerge with a significant energy offset.

On the other hand the acceptance of the channeling process is very small at LHC maximum energy. The critical angle is of the order of about 2.5 μrad at 7 TeV (i.e. maximum angle with respect to the crystalline planes to undergo channeling). Thus, the location of crystals in the lattice of the machine has to provide an angular distribution of impacting particles that is smaller than the critical angle to ensure stable channeling. The layout presented here allow to reach angular distributions below 1 μrad at 7 TeV. The possibility to build goniometers with sub-μrad resolution [17,18], made it possible to fulfill the required constraints on angular stability for crystal channeling at LHC maximum energy. However, experimental demonstration at such a high energy is mandatory.

3 Design goals and constraints

Various studies have been carried out to integrate a crystal test stand in the present betatron collimation system [19,20] for first feasibility tests. This requires addressing satisfactorily various aspects:

- A demonstration of crystal channeling with good efficiency of high energy hadron beams, up to 7 TeV.
- A demonstration that crystal collimation can improve the cleaning efficiency in the IR7-DS for both proton and lead ion beams, with respect to the present system.
- A comparison with respect to the performance of the present collimation system in the LHC, throughout the whole operational cycle.
- A validation of the energy scaling of coherent processes in bent crystals at the still unexplored LHC energy, and a confirmation of how cross-sections of nuclear point-like interactions in bent crystals evolve at such a high energy.

The final layout is based on two crystals installed in the IR7 betatron cleaning insertion of beam 1, for horizontal and vertical collimation tests. Horizontal and vertical crystals are

placed on the external and top side of the machine, respectively.

Other important constraints for the design, e.g. on longitudinal positions, come from space availability in the present collimation insertion, at locations where optics parameters are optimised for crystal collimation. To minimize impacts on the present tunnel infrastructure, crystals are mounted on standard collimator supports and use a similar fast plug-in technology [21]. Slots already equipped with collimator supports, prepared for future upgrades that will only be deployed beyond 2018, were available and therefore considered for installation. These longitudinal positions ensure also the presence of other infrastructure required, such as control cabling.

Other important considerations that were implicitly taken into account in the design work, which are not discussed in detail in this paper, are the need to minimize radiation to personnel during installation and later maintenance of the crystals and to ease fast interventions on the hardware. For example, if different installation locations provide similar performance, those at lower radiation doses are chosen.

4 Optimisation of crystal parameters and lattice position

Restrictions on available longitudinal positions, in connection with betatron settings of the full collimation chain, have a significant impact on crystal parameters. For example, the same cleaning efficiency could be achieved with different bending angles, provided that different betatron settings of the TCSGs are used to intercept the channeled halo particles. More subtly, rates of single diffractive events in crystals are related to the channeling efficiency, crystal length and beam loss in the IR7-DS. Ultimately, optimum combination of crystal parameters and installation position must ensure:

1. Improved cleaning performance in the IR7-DS compared to the present collimation system.
2. Interception of channeled halo particles with present secondary collimators with adequate margins from fixed magnet aperture.
3. Sufficient offset of the channeled beam at the selected TCSG, compared to the beam envelope defined by the crystal aperture.
4. Compatibility with crystal collimation tests at all beam energies, from 450 GeV up to 7 TeV.

4.1 Installation position

Semi-analytical tools based on linear beam transport have been developed to evaluate quickly feasibility of different crystal-based layouts. Using particle accelerator physics theory it is easy to demonstrate that, ideally, the best basic layout

consists of a crystal at a location with zero divergence and an absorber placed at $\pi/2$ phase advance, because of two main reasons: (1) a value of the Twiss parameter $\alpha \sim 0$, i.e. beam envelope parallel to closed orbit, can allow to move the crystal only linearly during the energy ramp, in order to maintain the channeling condition during adiabatic damping of the beam emittance. If $\alpha \neq 0$ the angular orientation of the crystal also has to vary accordingly to the beam envelope shrinking as a function of energy. (2) A phase advance ($\Delta\mu_{s-s_1}$) of about $\pi/2$ between the crystal and the selected collimator used to intercept the steered halo, ensures the maximum shift of such particles at the secondary collimation stage with respect to trajectories of unperturbed particles. The trajectory of particles experiencing an angular kick (θ) at s_1 can be described using the transfer matrix formalism. If a crystal is installed at s_1, and assuming $\alpha \sim 0$, the trajectory of a kicked particle is described by:

$$x(s) = \sqrt{\frac{\beta(s)}{\beta(s_1)}} \cos(\Delta\mu_{s-s_1})x(s_1)$$
$$+ \theta\sqrt{\beta(s)\beta(s_1)} \sin(\Delta\mu_{s-s_1}). \tag{1}$$

To fulfill the two conditions above, dedicated optics for the LHC-IR7 insertion would have to be produced. Even if this was possible with present magnet layout, the overhead for beam tests would become too large if new optics were to be commissioned. It was therefore decided to design optimized layouts for the existing and already commissioned IR7 optics [22]. After a first identification of suitable installation locations based on space and infrastructure availability, a sub-set of possible locations, crystal parameters, and collimator settings is determined based on semi-analytical tools.

Only the final layouts are discussed here, leaving for interested readers the detailed description of multiple layouts studied that can be found in [23]. Figures 4 and 5 show the trajectories followed by particles channeled (solid line) and scattered (dashed lines) at the crystal as a function of s, starting from 6 σ beam envelope, for the vertical and horizontal planes, respectively. Both injection (a) and maximum energy (b) cases are considered. The projection of collimator apertures on the plane of interest is also shown, together with the aperture model of the IR7 insertion. Several observations can be made:

- Positions close to $\alpha \sim 0$ are obtained (proximity to a plateau of the β function).
- At maximum energy the angular cut applied by the selected TCSG is about 5 μrad (i.e. all particles that acquired a deflection larger than 5 μrad due to the interaction with the crystal are intercepted by TCSG).
- At injection energy the angular cut applied by the selected TCSG is about 20 μrad.


(a)

(b)
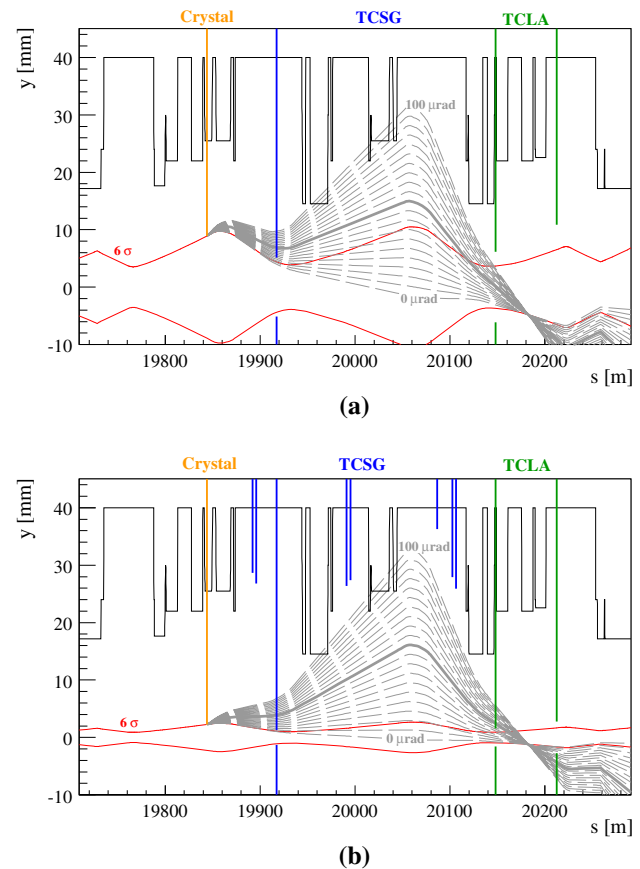
Fig. 4 Vertical trajectories of channeled halo particles (*solid gray line*) and mechanical aperture of the beam pipe (*black*) versus longitudinal position along the betatron cleaning insertion. The crystal, shown by the *orange line*, sits on the six betatron sigma beam envelope shown by the *red lines*. The *bold gray line* indicates a crystal kick of 50 μrad while the *dashed ones* range from zero to 100 μrad in 5 μrad steps. Injection **a** and 7 TeV **b** cases are given

4.2 Crystal bending angle

The maximum bending allowed corresponds to the maximum kick for which the trajectory of the deflected halo is never closer than a safe distance from the beam pipe. This distance is determined by considerations of possible uncertainties, beam parameters and aperture tolerances. Operational experience during the LHC Run 1 indicated that the aperture model used is adequate, the maximum shift of a closed orbit is below 2 mm, and the beta beating is below 10% [24]. Beams are dumped by the interlock system when a drift of a closed orbit of 2 mm is measured. Thus a conservative margin of 5 mm as the minimum distance between the trajectory of channeled halo particles and the beam pipe is taken.

For the vertical layout, the vertical TCSG used to intercept the channeled halo particles is upstream of the vertical aperture restriction. Thus, the channeled halo will be intercepted by such a TCSG before reaching unsafe distances from the magnets, at any energy.
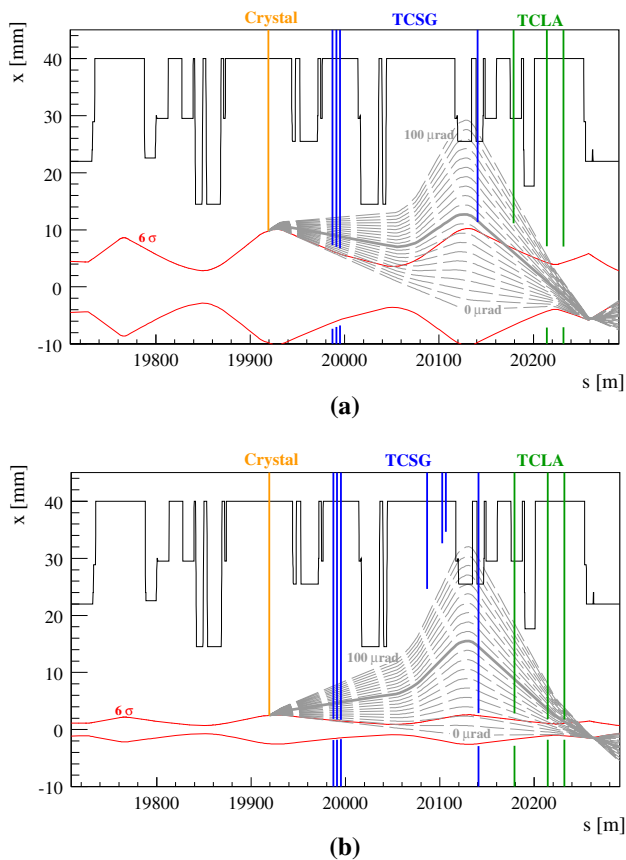
Fig. 5 Semi-analytical studies regarding the horizontal crystal location: **a** at 450 GeV, **b** at 7 TeV. The same notation as in Fig. 4, but applied to the *horizontal plane*

For the horizontal layout a similar situation is obtained using the collimator settings shown in Fig 5. However, at maximum energy it is possible to intercept the channeled particles by using only the last TCSG shown in Fig 4b. This configuration will allow tests with a minimal set of collimators in place, but poses a constraint on the maximum deflection allowed that is of about 65 µrad to avoid risks of touching the fixed magnet aperture.

For operation with circulating beams, one must take into account that repeated passages through the crystal, with angles slightly modified each time by the previous passage, can lead to channeling also when the crystal has a small tilt with respect to its optimal orientation. In the LHC with 7 TeV beams this tilt is found to be about 5 µrad from numerical simulation, i.e. slightly more than twice the critical angles at such an energy ($\theta_c \sim 2.5$ µrad), and also observed experimentally [1]. This tilt with respect to the beam envelope gives an additional deflection to channeled particles on top of the one given by the crystal bending. Even though any misorientation must be minimized for efficient crystal collimation, this additional kick must be taken into account to ensure machine safety during angular scans that will be performed

in experimental tests. Hence a margin has to be included in the final choice of requested bending. Thus, to perform safe angular scans at maximum energy a margin of $\sim 4\theta_c$ (i.e. ~ 10 µrad) is adopted. The maximum crystal bending allowed is therefore decreased to 55 µrad.

The minimum crystal bending is determined by requiring a confinement of the channeled beam on the TCSG front face, at injection energy. This minimum value can be evaluated by considering the crystal as a point-like source of the beam formed by the channeled halo [23,25]. The full spot size (σ_{ch}) on the absorber is given by the angular acceptance of the channeling process (i.e. the critical channeling angle θ_c):

$$\sigma_{ch} = 2\theta_c\sqrt{\beta(s_{Abs})\beta(s_{Cry})}\sin(\Delta\mu_{Abs-Cry}). \qquad (2)$$

At 450 GeV the critical angle is about 9.7 µrad. Thus, given the angular cut of 20 µrad provided by the selected TCSGs (see Sect. 4.1) a minimum bending of 30 µrad is needed for the full confinement of the channeled beam on the absorber front face. Taking into account the supplementary deflection due to the multi-turn process, a margin has to be included to ensure the full confinement during a complete angular scan. In contrast to the maximum energy case, the risk at injection energy is to channel halo particles when the total deflection given is not enough to reach the secondary collimator. Given the reduced risks for the machine safety at injection energy, a slightly relaxed margin of $\sim 3\theta_c$ (i.e. ~ 30 µrad) is adopted. Adding this margin to the angular cut provided by the selected TCSGs, the minimum bending required is therefore 50 µrad.

In conclusion, to ensure the full confinement of the extracted beam spot on the absorber and safe distance with respect to machine aperture at any energy and any layout configuration, the required crystal bending is in the range of 50−55 µrad.

4.3 Crystal length

The key parameters of a bent crystal are its length (l) and bending angle (θ), which define its bending radius (R) as $R = l/\theta$. The more crystals are bent (i.e. the smaller is R), the more particles are forced to oscillate in proximity to the crystalline planes, therefore increasing the probability of inelastic interactions with the nuclei. The minimum bending radius below which the potential well disappears and channeling is no longer possible is called the critical bending radius (R_c), and undesired nuclear interactions become predominant for bending radii $R < 3R_c$ [26]. Thus, bending radii $R > 3R_c$ were considered to provide a "smooth" particle steering needed to reduce as much as possible the probability of inelastic interactions. This condition calls for long crystals. On the other hand, the probability of inelastic interactions increases with the number of oscillations per-

Table 1 Critical channeling angle (θ_c), oscillation period (λ) and critical bending radius (R_c) for silicon crystals at typical energies of interest for our purpose

Energy (Gev)	θ_c (μrad)	λ (μm)	R_c (m)
450	9.7	61.9	0.8
6500	2.6	235.4	11.7
7000	2.5	244.3	12.6
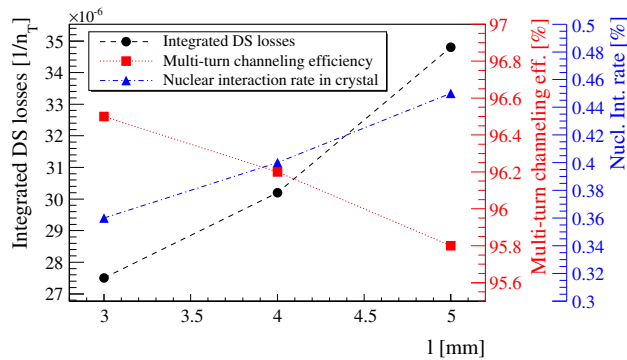
Fig. 6 Integrated losses in the beam 1 IR7-DS (*black*), multi-turn channeling efficiency (*red*) and nuclear interaction rate (*blue*) as a function of the crystal length for a fixed bending of 50 μrad. Integrated losses are normalised to the total number of particles intercepted by the crystal (n_T)

formed between crystalline planes, which is defined by the oscillation period (λ) [26]. These key parameters are reported in Table 1, for energies of our interest.

Moreover, the longer the path of particles between crystalline planes, the larger is the probability of elastic interactions that can let particles out from the channel (dechanneling process [26]). Such particles do not acquire the desired deflection. Thus, they can either arrive on the absorber with a reduced impact parameter, or even bypass it and be lost somewhere else in the ring. In both cases the cleaning performance of the system is jeopardised.

A compromise has to be found in order to decrease as much as possible the probability of nuclear interactions for channeled particles, without degrading too much the multi-turn channeling efficiency. Complete multi-turn tracking simulations (described in Sect. 6.1) were performed for different crystal lengths $l = (3, 4, 5)$ mm and $\theta = 50$ μrad. Key observables are: integrated losses in the IR7-DS, multi-turn channeling efficiency, and the nuclear interaction rate at the crystal. Such simulations were performed with nominal LHC optics at 7 TeV [22] and collimator settings which are reported in Table 3. The complete list of settings for all the collimators present in the LHC can be found in [23]. Taking as an example what is achieved with the final layout for the horizontal crystal using configuration 1 (see Sect. 5.3), the integrated losses in the IR7-DS, nuclear interaction rate and the multi-turn channeling efficiency are reported in Fig. 6.

These results provide a quantitative evaluation of the effects qualitatively introduced above. The variation of multi-turn channeling efficiency is found to be in the range of 1% for the three lengths compared. The variation of nuclear interaction rate is also small, and ranges from about the 0.36% with $l = 3$ mm to about 0.45% with $l = 5$ mm. The main difference is obtained for the IR7-DS integrated losses, where about 20% more losses are expected using $l = 5$ mm with respect to $l = 4$ mm. Thus, a crystal length of $l = 4$ mm is adopted to ensure the best system performance with a bending radius as large as possible, achieving $R > 6R_c$ at 7 TeV. Such a deflection in a so short a range is equivalent to having a uniform dipole field, ideally acting only on a selected portion of the 7 TeV beam halo, of about 310 T.

5 Final layout and configurations

5.1 Installation layout

The final crystal parameters and installation locations are reported in Table 2. In this section the proposed set of optimal collimator settings for beam tests at injection and maximum energy are presented (Table 3). Note that in addition to TCSGs that are used as absorbers, TCLAs must also be used. This because TCSGs are made of 1 m long jaws of CFC (carbon fibre-carbon composite) to intercept the channeled halo, which is not enough to completely absorb it and the physics debris will be mainly lost in the IR7-DS. This could mask possible improvements connected to the reduced inelastic interaction rate at the primary collimation stage. Thus, such debris is intercepted using the TCLAs that are made of 1 m long jaws of tungsten.

It was decided to test two technologies of crystal manufacturing. A strip crystal (ST) produced by Istituto Nazionale di Fisica Nucleare (INFN) [27,28] is installed in the horizontal plane, while a quasi-mosaic crystals (QM) produced by Petersburg Nuclear Physics Institute (PNPI) [29] in the vertical one. The main difference is given by the crystalline planes used to deflect the halo particles. In ST crystals the (110) planes are used, which are equidistant. In QM crystals the (111) planes are used, where a ratio 1:3 is present in the distance between subsequent planes. They are expected to be equivalent for proton beams. For heavy ion beams an increased probability of inelastic interactions is expected when ions are trapped in the smaller channel of QM crystals. Beam tests will address the influence of this difference between the two crystals by systematic comparisons of their performance.

5.2 Vertical configuration

The layout for the vertical case is shown in Fig. 7 for 450 GeV (a) and 7 TeV (b) beam energy. Such a final layout

Table 2 Installation position and main features of the crystals installed in the LHC (i.e. bending angle, length, material and crystal type). Optics parameters are also reported

Name	s (m)	Collimation plane	Bending (µrad)	Length (mm)	Mat.	Bending planes	β_x (m)	β_y (m)	α_x (rad)	α_y (rad)	D_x (m)	D_y (m)
TCPCH.A4L7.B1	19,919.24	Hor.	50	4	Si	110	341.03	65.36	−2.04	0.85	−0.37	−0.15
TCPCV.A6L7.B1	19,843.82	Ver.	50	4	Si	111	30.44	282.14	0.23	−2.63	0.14	−0.40

Table 3 Nominal settings at 7 TeV of the LHC collimation chain in the IR7, for the present system and in the case of crystals

Coll. name	Orient.	Setting (σ)	Setting (σ)	Setting (σ)
		Cry. H plane	Cry. V plane	Present coll.
TCPCH.A4L7.B1	Hor.	6	Out	Out
TCPCV.A6L7.B1	Ver.	Out	6	Out
TCP.	H/V/S	Out	Out	6
TCSG.	Skew	Out	Out	7
TCSG.D4L7.B1	Ver.	Out	7	7
TCSG.B4L7.B1	Hor.	7	Out	7
TCSG.A4R7.B1	Skew	7	Out	7
TCSG.A4L7.B1	Skew	7	Out	7
TCSG.6R7.B1	Hor.	7	Out	7
TCLA.	H/V	10	10	10

and collimator settings allow to perform tests at any energy with a minimal set of objects in place: one vertical crystal, the vertical TCSG.D4L7.B1 and the five TCLAs. Note that a TCLA collimator is available at 180° phase advance from TCSG.D4L7.B1. Thus, debris from the secondary collimator is automatically caught by the TCLA. A significant improvement of cleaning efficiency with respect to the present collimation system is expected using only these few collimators, as discussed in Sect. 6.

Using the nominal settings reported in Table 3, the mean impact parameters of the extracted halo and the transverse spot size at the selected TCSG are reported in Table 4.

5.3 Horizontal configuration

Two configurations were designed for the horizontal plane:

1. **One TCSG** Only the horizontal crystal, the last horizontal secondary collimator TCSG.6R7.B1 and the five TCLAs are used.
2. **Four TCSGs** The horizontal crystal, plus the TCSGs B4L7.B1, A4L7.B1, A4R7.B1 and 6R7.B1, plus the five TCLAs are used.

Configuration **1** is only suitable for tests at maximum energy, because at injection the channeled halo is not inter-
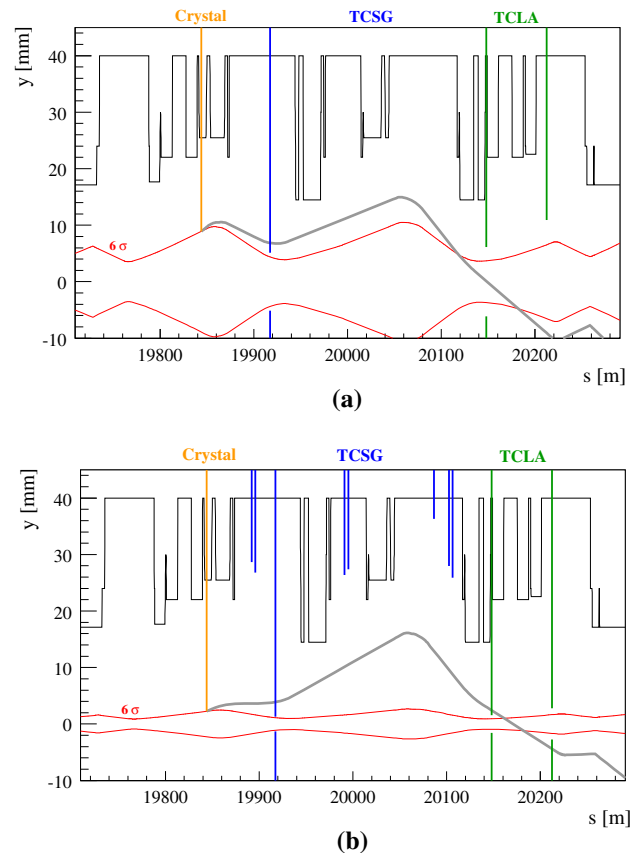
Fig. 7 Trajectory (*gray line*) of the channeled halo particles at 450 GeV (**a**) and 7 TeV (**b**), for a crystal bending angle of 50 µrad. Same notation as in Fig. 4

Table 4 Mean impact parameter ($\bar{y}_{ch}$) and spot full width (σ_x^{ch}, σ_y^{ch}) on the TCSG.D4L7.B1, for injection and maximum energy

Energy (Gev)	$\bar{y}_{ch}$ (mm)	σ_x^{ch} (mm)	σ_y^{ch} (mm)
450	1.8	9.5	1.2
7000	2.6	2.4	0.3

cepted by the TCSG.6R7.B1, as shown in Fig. 8a where it is represented by the last blue line. In the horizontal plane no optimum TCLA location to catch the debris from horizontal TCSGs is available. However, the absorption of the debris from the secondary collimator is ensured by the proximity to TCLAs.
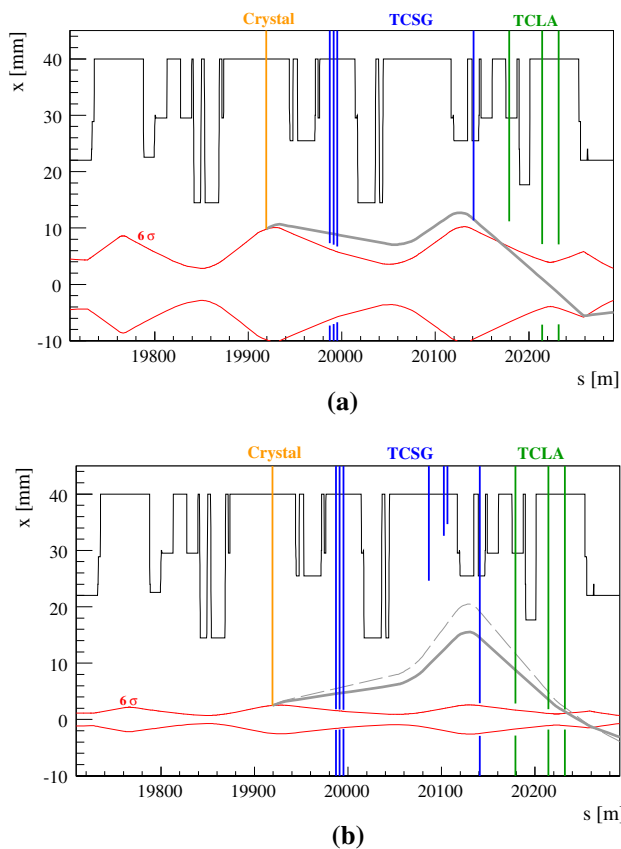
Fig. 8 Trajectory of the channeled halo particles at 450 GeV (**a**) and 7 TeV (**b**) using configuration **2**, for a crystal bending of 50 μrad. Same notation as in Fig. 4. The *dashed gray line* represents the maximum kick for which a minimum safety distance with respect to the magnet aperture is present, before reaching the TCSG.6R7.B1 using configuration **1**

Closing the horizontal TCSG.B4L7.B1 as in configuration **2**, allows interception of the full spot of the extracted beam halo at any energy, as shown in Fig. 8. However, the two subsequent skew collimators have also to be used to intercept the debris from the B4L7, which would otherwise be lost in the IR7-DS. The TCSG.6R7.B1 has to be in place anyway, because it is at the same phase advance of the TCSP in the LHC-IR6 (dump protection). Thus, its retraction could cause an overload of absorbed particles in the other collimator.

The mean impact parameters of the extracted halo and the transverse spot size at the selected TCSG are reported in Table 5, for the two configurations.

A significant improvement of cleaning efficiency compared to the present collimation system is expected using either of the two configurations (see Sect. 6). In conclusion, configuration **1** is optimized to demonstrate the feasibility of improved cleaning efficiency using only one bent crystal and a minimal set of standard collimators at maximum energy, while configuration **2** is suited to demonstrate improved cleaning throughout the whole operational cycle of the LHC.

Table 5 Mean impact parameter ($\bar{x}_{ch}$) and spot full width (σ_x^{ch}, σ_y^{ch}) for the two horizontal configurations, for injection and maximum energy

Energy (GeV)	Conf.	$\bar{x}_{ch}$ (mm)	σ_x^{ch} (mm)	σ_y^{ch} (mm)
450	1	–	–	–
7000	1	11.6	1.6	1.1
450	2	1.8	1.2	6.3
7000	2	2.7	0.3	1.9

6 Expected performance

An extensive simulation study was carried out to evaluate the expected performance of the crystal layouts proposed and compared with the present collimation system. Both injection and maximum energy were simulated. Considerations on possible further improvements of cleaning efficiency are discussed, mainly related to an optimised absorber for the channeled halo.

6.1 Simulation setup

Simulations were made using `SixTrack` [30–33] that allows a symplectic, fully chromatic and 6D tracking along the magnetic lattice of the LHC, taking into account interactions with the ring collimators and the detailed aperture model of the entire ring. The treatment of interactions between protons and bent crystals is carried out using a dedicated routine [20,23,34] implemented in `SixTrack`. The simulation setup allows estimation of the density of protons lost per metre with a resolution of 10 cm along the entire ring circumference, for a given halo intercepted and collimator settings. Losses on superconducting magnets, warm elements and collimators are indicated as cold, warm and collimator, respectively.

An example of simulated loss maps for the present collimation system is given in Fig. 10. It is clearly visible that the IR7-DS is the limiting location of the whole ring in terms of cleaning efficiency (i.e. where the highest losses are expected). The average level of protons lost per metre in the two clusters at this location (Q8-9 and Q10-11, respectively) defines the collimation performance of the system under study.

A sample of about 10^7 protons intercepted by the collimation system is used, in order to provide sufficient statistics to estimate losses of about 10^{-6}, which is the best performance achievable with the present secondary collimators used as absorber (as discussed in Sect. 6.3). Note that the results shown here are obtained using a perfect machine with nominal beam parameters and optics at 7 TeV and 450 GeV [22]. Thus, results should be considered as an optimistic performance estimate, but still provide a reliable comparison between the two methods. Nominal settings for the collima-
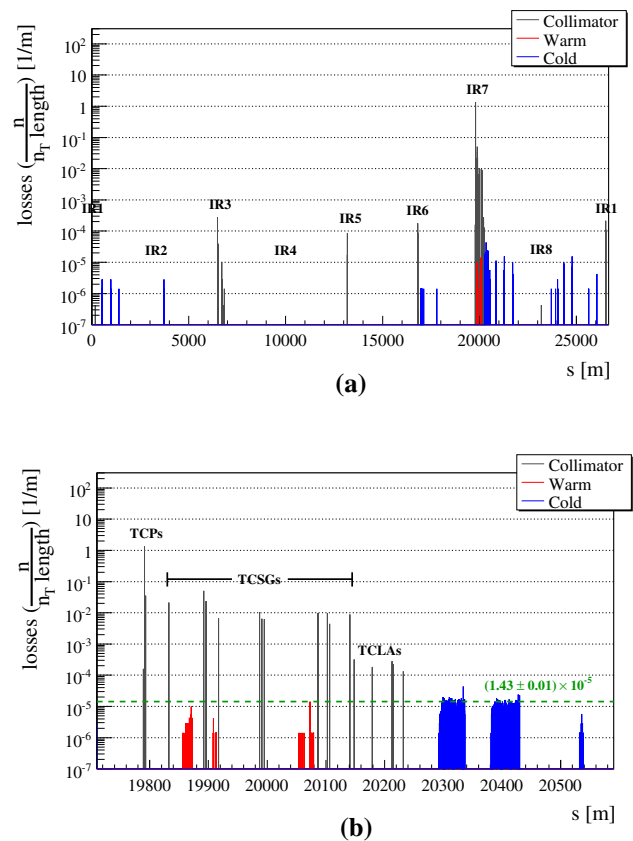
(a)

(b)
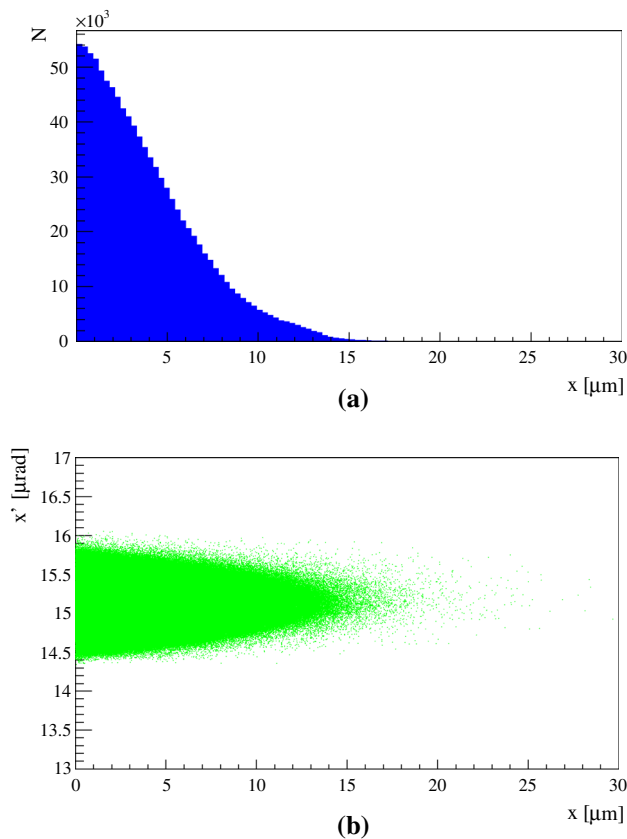
Fig. 9 Distribution of impact parameters on the crystal (**a**); phase space intercepted by the horizontal crystal at 7 TeV (**b**)

(a)

(b)

Fig. 10 Simulated beam loss pattern with the present collimation system and 7 TeV beams. The whole LHC (**a**), zoom of the IR7 insertion (**b**). The *dashed green line* shows the cleaning performance of the system, defined as the average level of protons lost in the IR7-DS. (1 p = 1.4×10^{-6} m^{-1})

tion chain are also used, reported in Table 3 (settings of the complete collimation system can be found in [23]).

Particular attention has been paid to the impact parameter and the angular spread of particles at the first passage at the crystal. While for standard primary collimators this is not a critical parameter, as results are stable in a wide range of values up to hundreds of µm [35], for crystals the initial distribution affects significantly the channeling efficiency. Impact parameters of the order of tenths of a µm are expected in the real machine [36]. However, simulations with such low values would be not feasible due to the computing time needed. Parametric studies have been performed to find the best compromise between computing time needed and stability of simulation results, using data collected on the SPS and its extraction line as benchmark [23]. The RMS of the simulated halo incident on the crystal is about 3 µm, with a maximum divergence of about 1.4 µrad, as shown in Fig. 9.

6.2 Simulation results at 7 TeV

An example of a loss map for the full LHC ring, simulated for the horizontal plane at 7 TeV with the present collimation system, is shown in Fig. 10. The performance of horizontal crystal collimation in configuration **1** is shown in Figs. 11 and 12, for a crystal in channeling and amorphous orientation, respectively. The case of amorphous orientation is simulated to predict the gain factors during angular scans, but also to illustrate the expected performance if the channeling were to be lost in a crystal collimation system.

At 7 TeV simulations predict an improvement by about a factor 10 compared to the present collimation system when crystals are in channeling orientation. Conversely, a factor about 3–4 worse performance is expected when crystals are in amorphous orientation. The difference between configurations **1** and **2** for the horizontal plane is given by the cut in angle applied by the selected TCSGs on particles scattered by the crystal, and by the absorption efficiency of what emerges from those TCSGs. Configuration **1** is about 50% better because debris from the only TCSG used is absorbed immediately by the TCLAs downstream. Moreover, in the configuration **2** a larger number of impacts on the TCSG edge and surface facing the circulating beam is present. These protons see a smaller active length of the absorber, causing
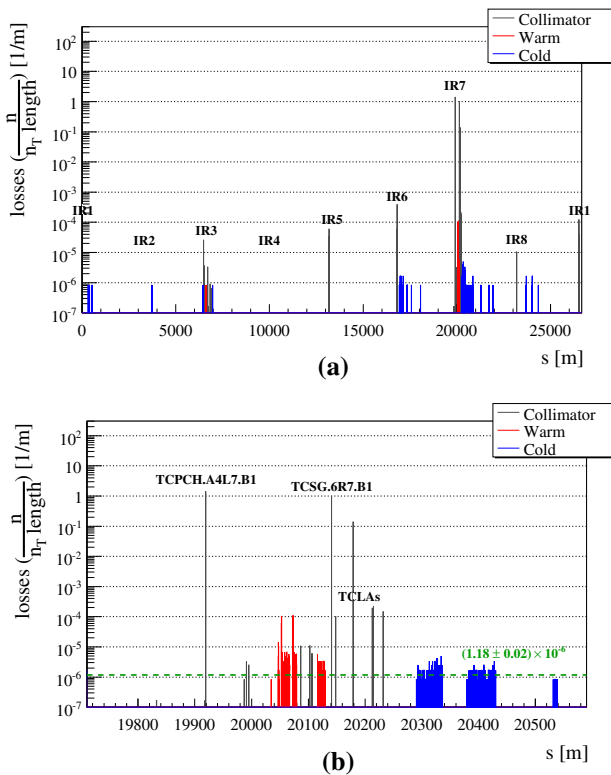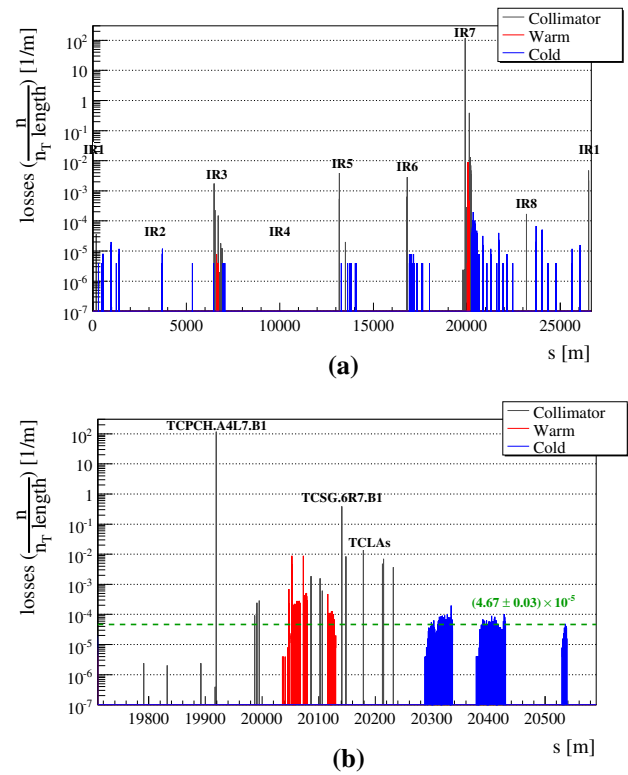
Fig. 11 Simulated beam loss pattern in the case of a horizontal crystal (config. **1**) in channeling orientation and 7 TeV beams. The whole LHC (**a**); zoom of the IR7 insertion (**b**). The *dashed green line* shows the cleaning performance of the system, defined as the average level of protons lost in the IR7-DS. (1 p = 8.3 $\times 10^{-7}$ m^{-1})

Fig. 12 Simulated beam loss pattern in the case of a horizontal crystal (config. **1**) in amorphous orientation and 7 TeV beams. The whole LHC (**a**), zoom of the IR7 insertion (**b**). The *dashed green line* shows the cleaning performance of the system, defined as the average level of protons lost in the IR7-DS. (1 p = 3.9 $\times 10^{-6}$ m^{-1})

a reduction of its absorption efficiency. A summary of simulated cleaning inefficiencies with the different systems and configurations is reported in Table 6.

The energy spectrum of off-momentum losses occurring in the IR7-DS in the case of horizontal standard collimation and configuration **1** with crystal in channeling, is shown in Fig. 13. As can be clearly seen in this figure, these losses are reduced both in amount and in deviation from the reference momentum. This is one of the key benefits of using a bent crystal as primary collimator, which leads to an overall reduction of off-momentum losses around the ring as is clearly visible by comparing Fig. 10a with Fig. 11a. This is also indicated by the fact that losses on the TCP in IR3 are significantly reduced. Some cold losses are present in IR3 of Fig. 11a, which are statistical fluctuations and are not significant (only one protons is lost in that bins).

In simulations with a crystal in an amorphous orientation, the density of protons lost in the crystal volume seems significantly above what is lost in a standard TCP. This is a feature of the normalisation to (m^{-1}). In particular when the crystal is misoriented with respect to the beam envelope, particles will pass through it many times before accumulating sufficient deflection to reach the TCSG apertures. Since TCPs are

Table 6 Summary table of average IR7-DS losses (i.e. cleaning inefficiency) at 7 TeV, for the present system (Std.) and crystal collimation (CH, AM, and for both horizontal configurations defined in Sect. 5.3)

Config.	Plane	IR7-DS average losses (10^{-6})	Gain w.r.t. std. coll.
Std.	H	14.3 ± 0.1	1.0
CH (1)	H	1.18 ± 0.02	12.3 ± 0.2
CH (2)	H	1.84 ± 0.07	7.8 ± 0.3
AM (1)	H	46.7 ± 0.3	0.31 ± 0.03
AM (2)	H	59.3 ± 0.09	0.24 ± 0.04
Std.	V	13.6 ± 0.1	1.0
CH	V	1.32 ± 0.02	10.3 ± 0.2
AM	V	48.0 ± 0.2	0.28 ± 0.02

made of carbon and crystals of silicon, they have similar radiation and interaction lengths. Thus, while accumulating the radiation length needed in a series of passages through the crystal to then impact on TCSGs, a similar interaction length seen in a single passage through a standard TCP is also accumulated. This leads to about the same number of particles experiencing deep inelastic interactions in the two objects (normalised to the total number of protons intercepted by the
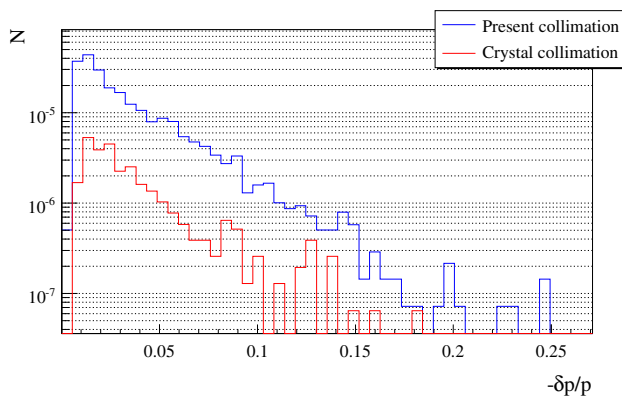
Fig. 13 Spectrum of energy offsets of particles lost in IR7-DS for standard horizontal collimation (*blue*) and configuration **1** with crystal in channeling (*red*)

Fig. 14 Integrated losses in the IR7-DS normalised to the total number of intercepted protons (*red*), for a horizontal crystal (config. **1**) with 50 μrad bending and different lengths. Contributions from interactions only with the crystal (*green*); contributions to losses generated after interacting also with TCSGs and/or TCLAs (*blue*)

system), and applying the normalisation to 1 m the factor 200 in lengths (60 cm of CFC for the TPCs, and 4 mm of silicon for crystals) is automatically translated to the height of the bar in the simulated loss maps. In conclusion losses in the plot are not representative of deposited energy in crystals, as the largest fraction of energy released will go in shower development outside the crystal. The main contribution to deposited energy in crystals is given by ionisation, which is about 2 MeV in 4 mm of silicon for 7 TeV protons.

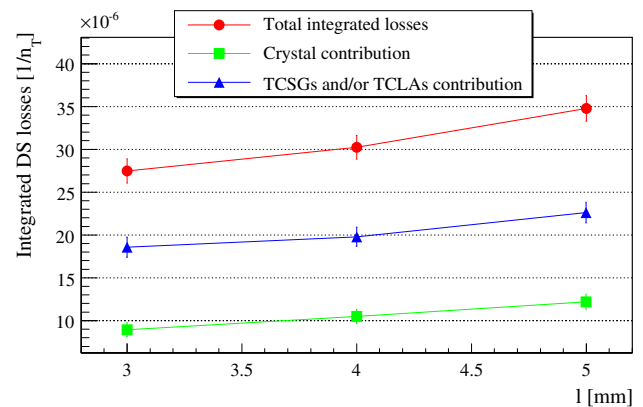### 6.3 Disposal of channeled halo particles

The present secondary collimators are made with a 1 m long carbon jaw that cannot efficiently dispose of the channeled halo beam. One can however understand, in simulations, the performance of a real crystal-based collimation system where new dedicated absorbers would be used.

Dedicated tools were developed to understand the source of losses in the IR7-DS. The main aim was to distinguish losses taking place after an interaction with the crystal only, from losses generated after interacting also with TCSGs and/or TCLAs. This allows to evaluate the contamination of losses in the IR7-DS due to debris from the absorbers.

The main outcome of these studies is shown in Fig. 14, taking into account the horizontal configuration **1** and different crystal lengths for a fixed bending of 50 μrad.

The energy spectrum of particles lost in IR7-DS are shown in Fig. 15 together with the interaction that led to such losses, for horizontal configuration **1** and optimal crystal parameters.

From these two figures it is clear that a significant contamination due to losses generated from interactions in the TCSGs and TCLAs is present. Thus, the development of a dedicated massive absorber could lead to even better cleaning performance of the crystal collimation system. Assuming an ideal absorber (i.e. black body) a factor about 3 could be
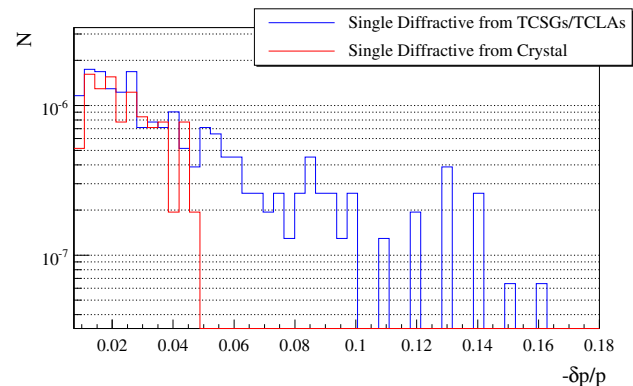

Fig. 15 Spectrum of energy offsets of particles lost in IR7-DS for horizontal configuration **1** with a crystal in channeling orientation

gained, leading to about a factor 30 better cleaning than the present system.

6.4 Simulation results at 450 GeV

Even if the present system is fully adequate for the LHC at injection energy, it is important to simulate the performance of the proposed crystal collimation layout in view of the first beam tests at such energy. This because it is easier to get beam time at injection energy, and tests at maximum energy depend on the results obtained at 450 GeV. Thus, it is important to have a layout that can demonstrate crystal channeling at this energy.

As can be clearly seen from Figs. 4a and 5a the effectiveness of kicks given by the crystals is significantly reduced compared to 7 TeV (Figs. 4b, 5b). Thus, the effect of losses generated by debris from TCSGs and TCLAs is more prominent at injection energy, because most of the intercepted particles are incident with a very small impact parameter. Dedicated settings must be used, and are reported in Table 7
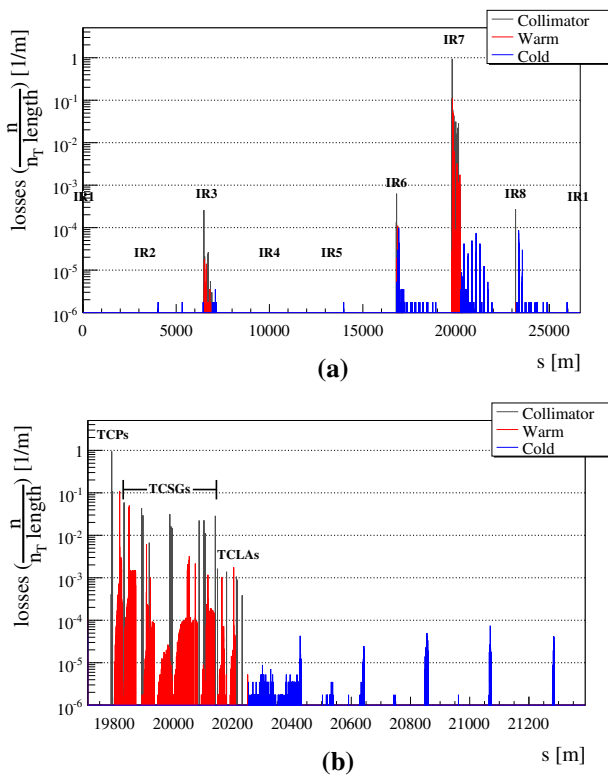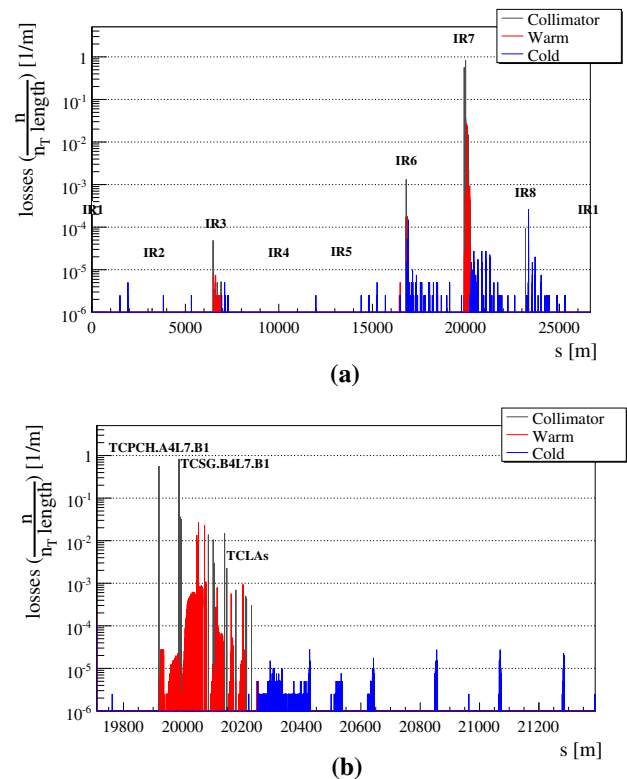
Fig. 16 Simulated beam loss pattern with the present collimation system and 450 GeV beams. The whole LHC (**a**), zoom of the IR7 insertion (**b**). (1 p = 1.2 $\times 10^{-6}$ m^{-1})

Table 7 Dedicated settings of IR7 collimators for comparative tests of different collimation systems at 450 GeV. For crystal collimation the IR7-TCSGs in place are all those downstream of D4L7.B1 and B4L7.B1 for vertical and horizontal configurations, respectively

Coll. name	Orient.	Setting (σ)	Setting (σ)	Setting (σ)
		Cry. H plane	Cry. V plane	Pres. coll.
CRY.H	Hor.	5.7	Out	Out
CRY.V	Ver.	Out	5.7	Out
TCP.	H/V/S	Out	Out	5.7
TCSG.	H/V/S	6.7	6.7	6.7
TCLA.	H/V	10	10	10

(settings of the complete collimation system can be found in [23]).

Examples of beam loss patterns simulated at injection energy are shown in Figs. 16 and 17 for the present collimation system and a crystal in channeling orientation, respectively. Losses occurring on superconducting magnets are present in more locations of the ring with crystal collimation than with the present system. However, most of them are due to debris from standard collimators, due to the reduced impact parameter, and not to interactions with the crystal. Also note that the IR7-DS is not the limiting location as for the 7 TeV case. Many other peaks are present between IR7 and IR8 that are more populated than the IR7-DS. Clean-

Fig. 17 Simulated beam loss pattern in the case of a horizontal crystal (config. **2**) in channeling orientation and 450 GeV beams. The whole LHC (**a**); zoom of the IR7 insertion (**b**). (1 p = 2.5 $\times 10^{-6}$ m^{-1})

ing about 20% worse is expected in IR7-DS with crystals in channeling compared to the present system. Conversely, improved performance is observed in the highest peaks of losses between IR7 and IR8, in a range between 60 and 80% depending on the peak. A significant increase of losses just after the TCT collimator in IR8 is expected when crystals in channeling are used. These losses are due to debris from TCSG and TCLA collimators, and are not an issue because they are well below the quench limit at this energy (estimated to be above 10^{-3}(m^{-1})). Similar simulation results are obtained for the vertical plane. In conclusion, tests at 450 GeV can certainly be used to establish and study channeling, but cannot be used for a direct demonstration that crystal collimation can improve the cleaning of the present system.

7 Conclusions

A system for crystal collimation studies at the LHC has been designed. The proposed layout includes two crystals to be installed on beam 1, for horizontal and vertical halo cleaning. Intercepting the channeled halo can be achieved with existing LHC collimators. This minimum system, which fulfills satisfactorily the requirements and design goals defined to demonstrate crystal collimation, has been actually installed in the LHC betatron cleaning insertion in 2014. Crystal tests

started in 2015. According to detailed simulations performed to address the cleaning performance of this system, not only will it allow reliable observation of channeling in all relevant LHC configuration, but also the demonstration that crystals could improve LHC halo cleaning.

The first observation of crystal channeling in the LHC with proton beams at both 450 GeV and at the record energy of 6.5 TeV was successfully obtained in 2015 [1]. This gives an adequate confidence level on the quality of the design conceived and its deployment. Dedicated tests were carried out in 2016 to probe the expected improvements of cleaning performance with respect to the present collimation system. Promising results were observed during the experiment, which are in agreement with expectations [37]. The detailed off-line analysis is still on-going.

References

1. W. Scandale, G. Arduini, M. Butcher, F. Cerutti, M. Garattini, S. Gilardoni, A. Lechner, R. Losito, A. Masi, D. Mirarchi et al., Phys. Lett. B **758**, 129 (2016)
2. R. Assmann, M. Magistris, O. Aberle, M. Mayer, F. Ruggiero, J. Jiménez, S. Calatroni, A. Ferrari, G. Bellodi, I. Kurochkin et al., The final collimation system for the LHC. Tech. rep. (2006)
3. G. Valentino, R. Bruce, M. Fiascaris, H. Garcia, P. Hermes, A. Mereghetti, D. Mirarchi, R. Kwee, E. Quaranta, S. Redaelli, et al., in *LHC Beam Operations Workshop* (2015)
4. D. Mirarchi, R. Bruce, M. Fiascaris, H. Garcia, P. Hermes, A. Mereghetti, R. Kwee, E. Quaranta, S. Redaelli, B. Salvachua, et al., in *LHC Beam Operations Workshop* (2016)
5. G. Apollinari, CERN Yellow Rep. **5**, 1 (2016)
6. B. Alonso, L. Rossi, Hilumi lhc technical design report. Tech. rep., CERN-ACC-2015-0140 (2015)
7. Hl-lhc preliminary design report: Fp7 hilumi lhc deliverable d1.5. Tech. rep., CERN-ACC-2014-0300 (2014)
8. G. Arduini, J. Barranco, A. Bertarelli, N. Biancacci, R. Bruce, O. Brüning, X. Buffat, Y. Cai, L. Carver, S. Fartoukh et al., J. Instrum. **11**(12), C12081 (2016)
9. S. Redaelli, R. Appleby, A. Bertarelli, R. Bruce, J. Jowett, A. Lechner, R. Losito, The high luminosity large hadron collider: the new machine for illumination the mysteries of the universe. ed. by R. Lucio, B. Oliver, vol. 1, pp. 215–241. World Scientific Publishing Co. Pte. Ltd., Singapore (2015). ISBN# 9789814675475
10. W. Scandale, G. Arduini, R. Assmann, C. Bracco, S. Gilardoni, V. Ippolito, E. Laface, R. Losito, A. Masi, E. Metral et al., Phys. Lett. B **692**(2), 78 (2010)
11. W. Scandale, G. Arduini, R. Assmann, C. Bracco, F. Cerutti, J. Christiansen, S. Gilardoni, E. Laface, R. Losito, A. Masi et al., Phys. Lett. B **703**(5), 547 (2011)
12. W. Scandale, G. Arduini, R. Assmann, F. Cerutti, S. Gilardoni, E. Laface, R. Losito, A. Masi, E. Metral, D. Mirarchi et al., Phys. Lett. B **714**(2), 231 (2012)
13. W. Scandale, G. Arduini, M. Butcher, F. Cerutti, S. Gilardoni, L. Lari, A. Lechner, R. Losito, A. Masi, A. Mereghetti et al., Phys. Lett. B **726**(1), 182 (2013)
14. W. Scandale, G. Arduini, R. Assmann, C. Bracco, F. Cerutti, J. Christiansen, S. Gilardoni, E. Laface, R. Losito, A. Masi et al., J. Instrum. **6**(10), T10002 (2011)
15. P. Hermes, R. Bruce, J. Jowett, S. Redaelli, B.S. Ferrando, G. Valentino, D. Wollmann, Nuclear instruments and methods in physics research section A: accelerators. Spectrom. Detect. Assoc. Equip. **819**, 73 (2016)
16. N.F. Mounet, Impedance. LHC Collim. Rev. (2013). https://indico. cern.ch/event/251588/session/1/contribution/6/material/slides/0. pdf
17. M. Butcher et al., High precision piezo goniometer for LHC crystal experiment. http://indico.cern.ch/event/355809/session/1/ contribution/6/material/slides/0.pdf
18. M. Butcher, A. Giustiniani, R. Losito, A. Masi, in *Industrial Electronics Society, IECON 2015-41st Annual Conference of the IEEE*, pp. 003887–003892 (IEEE, New York, 2015)
19. R. Assmann, S. Redaelli, W. Scandale, Optics study for a possible crystal-based collimation system for the LHC. Tech. rep. (2006)
20. V. Previtali, Performance evaluation of a crystal-enhanced collimation system for the LHC. Ph.D. thesis, EPFL These N.4794, CERN-THESIS-2010-133 (2010)
21. T. Weiler, O. Aberle, R. Assmann, R. Chamizo, Y. Kadi, J. Lettry, R. Losito, S. Redaelli, in *2007 IEEE Particle Accelerator Conference (PAC)*, pp. 1625–1627 (IEEE, New York, 2007)
22. O. Brüning, et al., *LHC design report, Optics and Single Particle Dynamics* (European Organization for Nuclear Research, Switzerland, 2004)
23. D. Mirarchi, Crystal collimation for lhc. Ph.D. thesis, Imperial Coll., London, CERN-THESIS-2015-099 (2015)
24. R. Bruce, S. Redaelli, J. Wenninger, M. Giovannozzi, R. De Maria, S. Fartoukh, R. Tomas, Parameters for hl-lhc aperture calculations and comparison with aperture measurements. Tech. rep. (2014)
25. W. Scandale, D. Mirarchi, S. Redaelli, in *Proceedings of IPAC* (2013)
26. V. Biryukov, Y. Chesnokov, K. V.I, *Crystal channeling and its application at high energy accelerators* (Springer, Berlin, 1996)
27. V. Guidi, L. Lanzoni, A. Mazzolari, J. Appl. Phys. **107**(11), 113534 (2010)
28. S. Baricordi, V. Guidi, A. Mazzolari, D. Vincenzi, M. Ferroni, J. Phys. D Appl. Phys. **41**(24), 245501 (2008)
29. Y.M. Ivanov, A. Petrunin, V.V. Skorobogatov, J. Exp. Theor. Phys. Lett. **81**(3), 99 (2005)
30. F. Schmidt, SixTrack, User's reference manual. Tech. rep., CERN SL/94-56 (AP) (1994)
31. http://sixtrack.web.cern.ch/SixTrack/
32. G. Robert-Demolaize, R. Assmann, S. Redaelli, F. Schmidt, in *Proceedings of the Particle Accelerator Conference, 2005. PAC 2005*, pp. 4084–4086 (IEEE, New York, 2005)
33. http://lhc-collimation-project.web.cern.ch/lhc-collimation-project/code-tracking-2012.php
34. D. Mirarchi, G. Hall, S. Redaelli, W. Scandale, Nucl. Instrum. Methods Phys. Res. Sect. B Beam Interact. Mater. Atoms **355**, 378 (2015)
35. R. Bruce, R. Assmann, V. Boccone, C. Bracco, M. Brugger, M. Cauchi, F. Cerutti, D. Deboy, A. Ferrari, L. Lari et al., Phys. Rev. Spec. Topics Accel. Beams **17**(8), 081004 (2014)
36. G. Valentino, R. Aßmann, R. Bruce, F. Burkart, V. Previtali, S. Redaelli, B. Salvachua, G. Stancari, A. Valishev, Phys. Rev. Spec. Topics Accel. Beams **16**(2), 021003 (2013)
37. D. Mirarchi, R. Rossi, S. Redaelli, W. Scandale, in *6th HL-LHC Collaboration Meeting* (2016)